



## Special Feature: Design of High-power Lithium-ion Batteries with Long Operational Life

Research Report

### Impedance Analysis Using Symmetric Cells for Understanding Electrochemical Behaviour of Porous Electrodes for Lithium-ion Batteries

Nobuhiro Ogihara and Yuichi Itou

Report received on Aug. 9, 2017

**■ABSTRACT■** A detailed understanding of the electrochemical behaviour of the internal resistance at the interface between porous electrodes and electrolytes for lithium-ion batteries leads to an ideal device design with high performance that simultaneously achieves high energy and high power density. Here we propose a novel analytical approach of determining the internal resistance that combines transmission line model theory for cylindrical pores and electrochemical impedance spectroscopy using symmetric cells. The individual internal resistance components of the actual porous electrode/electrolyte interface obtained can be described as the following four parameters: electrical resistance ( $R_e$ ), electrolyte bulk resistance, ( $R_{sol}$ ), ionic resistance in pores ( $R_{ion}$ ), and charge-transfer resistance for lithium intercalation ( $R_{ct}$ ). We have succeeded in separating the four internal resistances at the porous electrode using the proposed combined electrochemical analysis.

**■KEYWORDS■** Lithium-ion Battery, Porous Electrode, Electrochemical Impedance Spectroscopy, Transmission Line Model, Thickness, Resistance

#### 1. Introduction

In lithium-ion batteries for automotive applications, high-power performance is required, especially for cells with high energy density using thick electrodes. The internal resistance of the electrode/electrolyte interface strongly influences the power capability. Elements that influence the internal resistance are the electrode and electrolyte materials, and structural factors including thickness, composition, and porosity, which affect tortuosity. As shown in **Figs. 1(a)** and **(b)**, the actual electrodes of lithium-ion cells have several types of porous structures consisting of a mixture of active material, carbon-conducting agent, and binder. As shown in **Fig. 1(c)**, the internal resistances at the porous electrodes can be expressed by four parameters: electric resistance ( $R_e$ ), electrolyte bulk resistance ( $R_{sol}$ ), ionic resistance in pores ( $R_{ion}$ ), and charge-transfer resistance for lithium intercalation ( $R_{ct}$ ).

Analysis using electrochemical impedance spectroscopy (EIS) and an equivalent circuit, like those shown in **Fig. 2**, is a useful method for investigating the internal resistance of devices such as Li-ion batteries<sup>(1-3)</sup> and electric double-layer capacitors,<sup>(4-10)</sup> as well as other electrochemical systems like porous

Ni electrodes for hydrogen production.<sup>(11,12)</sup> Many studies concerning the equivalent circuit of the internal resistance behavior for actual electrodes have only reported the apparent charge-transfer resistance ( $R_{ct, app}$ ) obtained by assuming a simple “planar” electrode/electrolyte interface, which considers a parallel circuit of resistance and capacitance as a semicircle (**Fig. 2(a)**).<sup>(13-16)</sup> However, it is difficult to fully explain the power capability of actual Li-ion batteries using only  $R_{ct, app}$  because the electrochemical processes at the porous electrode exhibit a time distribution such as that shown in **Figs. 2(b)** and **(c)**.

We recently proposed a new analytical approach, which is a combination of a theory based on the transmission line model (TLM) for cylindrical pores and an EIS analysis technique using symmetric cells (EIS-SC).<sup>(17,18)</sup> TLM has been widely used to describe such porous electrodes as a cylindrical pore for both faradaic (ideally polarized electrode, **Fig. 2(b)**)<sup>(4-9)</sup> and non-faradaic (ideally non-polarized electrode, **Fig. 2(c)**)<sup>(19-25)</sup> processes. TLM for cylindrical pores is applied either to estimate Nyquist plot profiles or to find individual internal resistances by fitting experimental data. In the EIS-SC technique, two identical electrodes are prepared at the same potential before measurement and used as both electrodes in the symmetric cell.

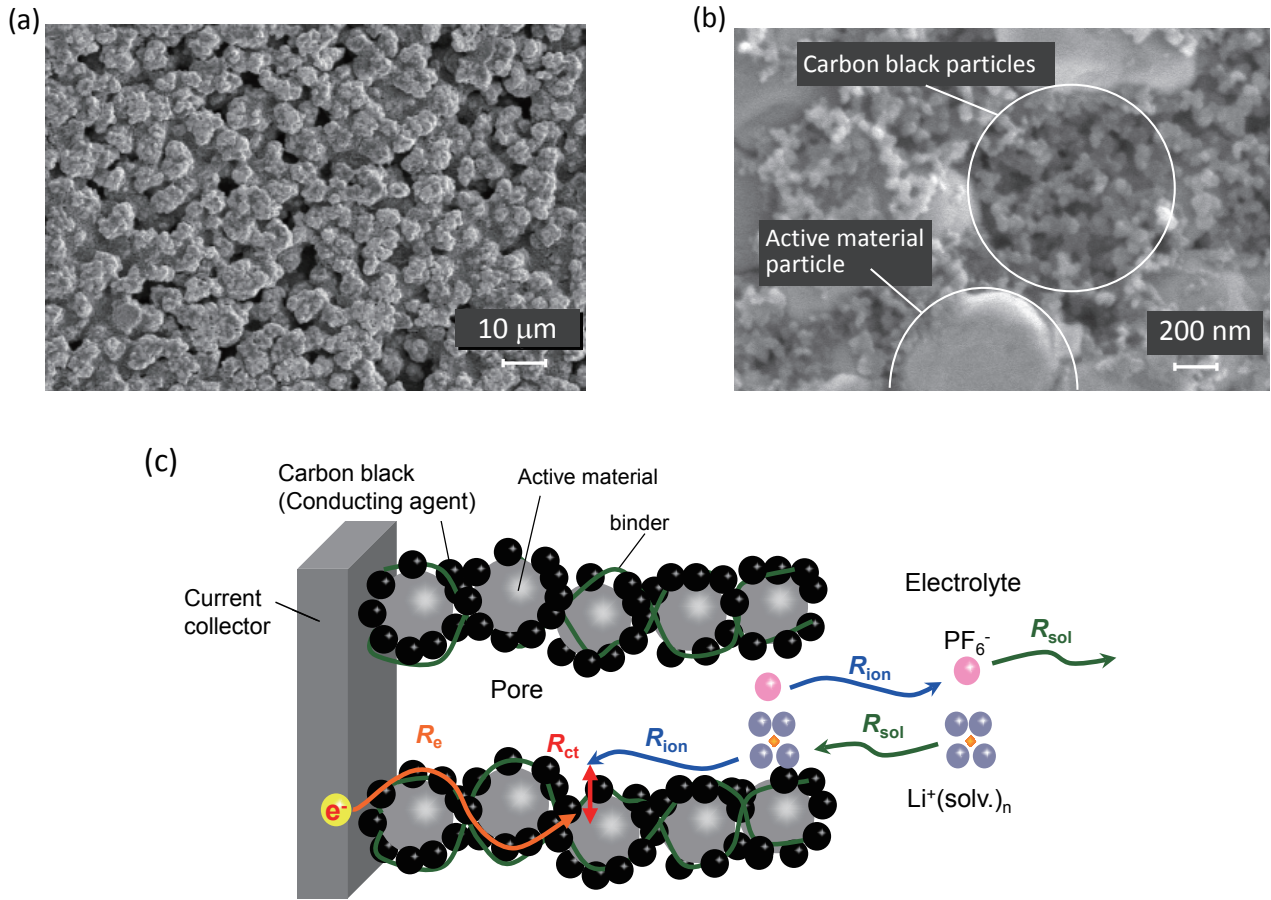


**Fig. 1** (a), (b) SEM images of the LiNiO<sub>2</sub>-based positive electrode surface. (c) Schematic illustration of respective internal resistances at porous electrodes for lithium-ion batteries.

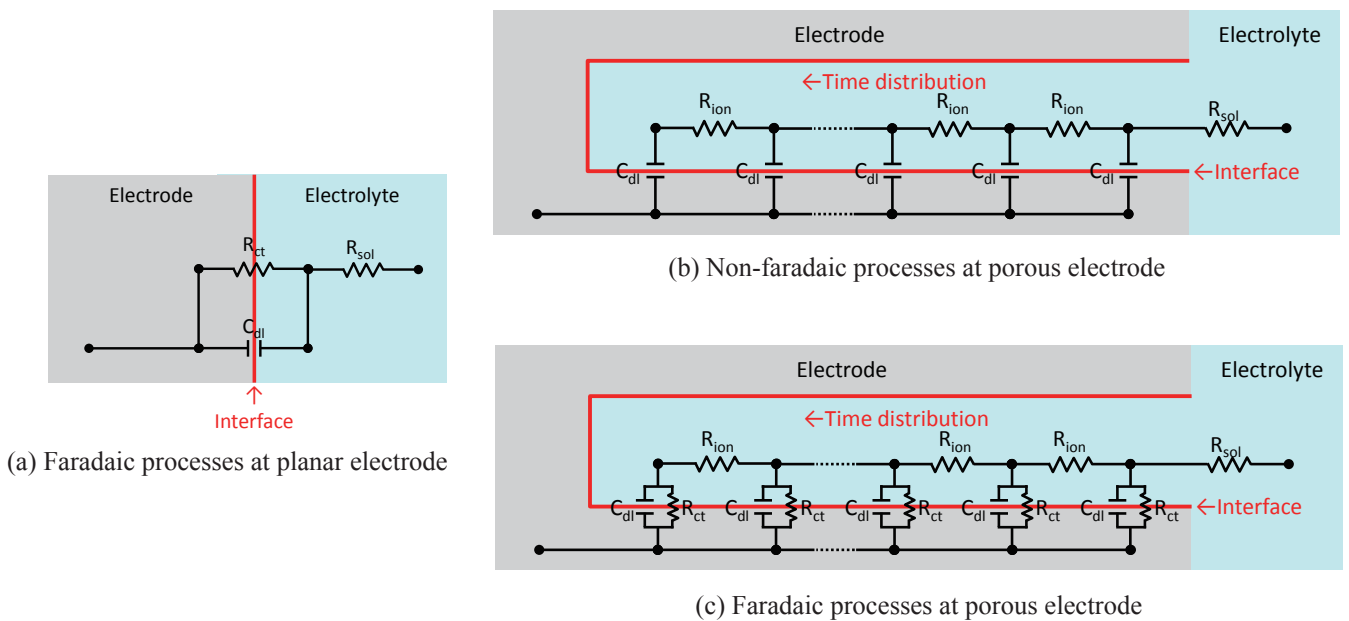


**Fig. 2** Schematic representations of electrode structures and their equivalent circuit models.

In conventional EIS measurements for positive or negative electrodes, lithium metal is often used as a counter electrode. The resulting impedance spectrum includes the impedance behavior of the lithium-metal electrode and consequently gives a mixed impedance profile ( $Z(\omega) = Z_+(\omega) + Z_{Li}(\omega)$ ), as shown in Fig. 3(a); therefore, these EIS measurements are not suitable for expressing the accurate internal resistance of the actual porous electrode. In contrast to the conventional EIS, EIS-SC provides the impedance spectra of the true electrode/electrolyte interface without interference from counter electrodes ( $Z(\omega) = 2Z_+(\omega)$ ), as illustrated in Fig. 3(b) and (c).

In this study, we first introduce the basic idea and interpretation of the proposed combined analysis and then discuss the results of temperature dependence for internal resistances. In particular, we believe that lithium-ion movement in the electrolyte-filled pores influences the internal resistance in the thick electrodes

(to be discussed in detail in the next paper). When a charge-transfer reaction occurs, the charge-transfer resistance has been often interpreted to include the ionic resistance in pores. In order to consider the internal resistance independently, those two resistances should be distinguished.

## 2. Impedance Theory for Cylindrical Pores according to the Transmission Line Model (TLM)

For non-faradaic (Fig. 2(b)) and faradaic (Fig. 2(c)) processes at porous electrodes, the overall impedance is expressed as Eqs. (1) and (2), respectively.<sup>(19,20,25)</sup>

$$Z_{non-faradaic} = \sqrt{\frac{R_{ion,L}}{j\omega C_{dl,A} \cdot 2\pi r}} \coth \sqrt{R_{ion,L} \cdot j\omega C_{dl,A} \cdot 2\pi r L} \quad (1)$$

$$Z_{faradaic} = \sqrt{\frac{R_{ion,L} \cdot R_{ct,A}}{(1 + j\omega R_{ct,A} \cdot C_{dl,A}) \cdot 2\pi r}} \coth \sqrt{\frac{R_{ion,L} \cdot (1 + j\omega R_{ct,A} \cdot C_{dl,A}) \cdot 2\pi r}{R_{ct,A}}} L \quad (2)$$

The limiting values of the real ( $Z'_{\omega}$ ) as  $\omega \rightarrow 0$  in non-faradaic and faradaic processes are shown in Eqs. (3) and (4), respectively.

$$Z'_{non-faradaic, \omega \rightarrow 0} = \frac{R_{ion}}{3}, \quad (3)$$

$$Z'_{faradaic, \omega \rightarrow 0} = \frac{R_{ion}}{3} + R_{ct}, \quad (4)$$

where  $R_{ion}$  is the mobility of Li ions inside the porous electrodes. From these mathematical equations,  $R_{ion}$  can be expressed as shown in Eqs. (5) and (6).

$$R_{ion} = R_{ion,L} \times \frac{L}{n}, \quad (5)$$

$$R_{ion,L} = \frac{\rho}{\pi r^2}, \quad (6)$$

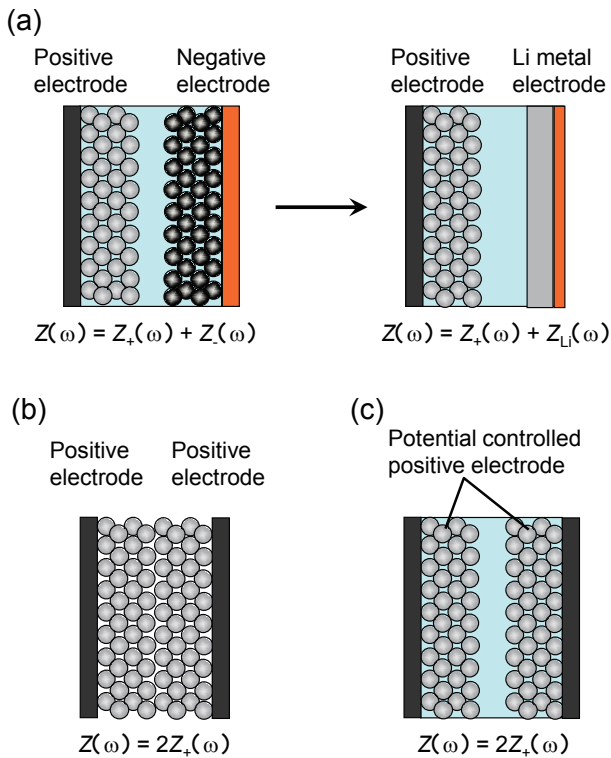


**Fig. 3** Schematic cell configurations: (a) asymmetric cell for conventional and classical impedance measurements, (b) symmetric cell without separator including electrolyte for electric resistance ( $R_e$ ) measurements, and (c) symmetric cell with separator including electrolyte for ionic resistance in pores ( $R_{ion}$ ) and charge-transfer resistance of lithium intercalation reaction ( $R_{ct}$ ) measurements.

where  $R_{ion,L}$  is the ionic resistance per unit pore length. In addition,  $R_{ct}$  is expressed as Eq. (7).

$$R_{ct} = \frac{R_{ct,A}}{2\pi rL}, \quad (7)$$

where  $R_{ct,A}$  is charge-transfer resistance per unit electroactive surface area. Using this combined approach, we have succeeded in separating the individual electrochemical parameters and corresponding kinetic interpretation from the temperature dependence.

Nyquist plots for non-faradaic processes calculated using Eq. (1) are shown in Fig. 4(a) for various  $R_{ion}$  values. The plot is linear with a 45-degree slope from the real axis in the high-frequency region and transitions to a constant  $Z''_{\omega}$  value in the low-frequency region. The length of the straight line with a slope of 45° in the high-frequency region increases with increasing  $R_{ion}$ . In contrast, as shown in Fig. 4(b), Nyquist plots for faradaic processes calculated using Eq. (2) for various  $R_{ct}$  values show linearity with a 45-degree slope from the real axis in the high-frequency region and semicircle behavior in the low-frequency region. When  $R_{ct}$  is increased to large values, the Nyquist plot calculated using Eq. (2) becomes similar to that calculated using Eq. (1).

### List of Symbols

$L$	unit pore length, cm
$r$	pore radius, cm
$\rho$	electrolyte resistance, $\Omega\text{cm}$
$S$	electrode surface area, $\text{cm}^2$
$n$	number of pores per unit electrode surface area
$C_{dl,A}$	electric double-layer capacitance per unit electroactive surface area, $\text{F cm}^2$
$C_{dl}$	total electric double-layer capacitance ( $C_{dl} = C_{dl,A} 2\pi rL$ ), F

### 3. Impedance of Porous Electrodes of the Symmetric Cell

The symmetric cell (Fig. 3(c)) results for  $\text{LiNiO}_2$ -based positive electrodes, which are composed of  $\text{LiNi}_{0.75}\text{Co}_{0.15}\text{Al}_{0.05}\text{Mg}_{0.05}\text{O}_2$ , carbon black conducting agent, and polyvinylidene fluoride binder (85:10:5 weight ratio), with SOC=0 and 50% were characterized as being due to non-faradaic and faradaic processes,

respectively. The experimental results of the Nyquist plots at SOC = 0 (Fig. 5(a)) and 50% (Fig. 5(b)) are in agreement with theory, as shown in Figs. 4(a) and (b), respectively. At SOC = 0%, the Nyquist plot shows a typical electrical blocking behavior. This behavior suggests that only the formation of an electric double layer capacitor occurs. No charge-transfer reactions (i.e. lithium intercalation) occur at the interface despite using the charge-transfer-active  $\text{LiNiO}_2$  electrode. This result reflects the lithium-ion conduction in the bulk

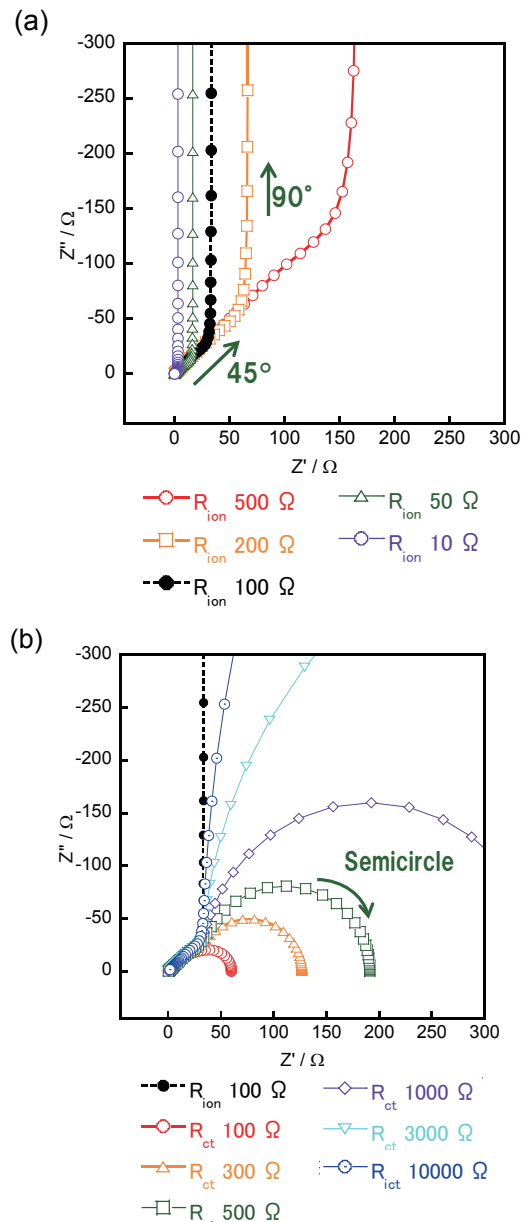


**Fig. 4** Simulated Nyquist plots for a cylindrical pore,  $L = 1$  cm,  $r = 0.5$  cm,  $C_{dl} = 0.1$   $\text{mF cm}^{-2}$ , as predicted by: (a) Non-faradaic processes calculated from Eq. (1) and (b) Faradaic processes calculated from Eq. (2) when using the listed values.

electrolyte and in the electrolyte-filled pores, which are expressed as the electrolyte bulk resistance ( $R_{sol}$ ) and the ionic resistance in pores ( $R_{ion}$ ), respectively. While the Nyquist plot at SOC = 50% (Fig. 5(b)) is almost the same as that seen for SOC = 0% (Fig. 5(a)) in the frequency region greater than 20 Hz, the plot appears as a semicircle at low frequencies. The Nyquist plot contains information on  $R_{sol}$  and  $R_{ion}$  in the high-frequency region as well as the charge-transfer resistance for the lithium-intercalation reaction ( $R_{ct}$ ) in the low-frequency region. The overlap of the Nyquist plots in the high-frequency region for SOC = 0 and 50% is an interesting and important experimental result. This result suggests that  $R_{ion}$  exists independently and can be separated using the results from  $R_{ct}$  in the porous electrodes for faradaic processes.

#### 4. Temperature Dependence of Individual Internal Resistances of Porous Electrodes

The temperature dependence of Nyquist plots is used to build a kinetics interpretation of the individual internal resistances. **Figures 6(a)** and **(b)** show the temperature dependence of Nyquist plots at SOC = 0%

and 50%, respectively, at temperatures between 10 and 60°C. In the Nyquist plots at SOC = 0% (Fig. 6(a)), with decreasing temperature, the real impedance component at 100 kHz, which determines the value of  $R_{sol}$ , shifts toward more positive values, and the length of the 45-degree-slope line, which reflects  $R_{ion}$ , increases. This indicates that these two internal resistances gradually increase with decreasing temperature. In the Nyquist plots at SOC = 50% (Fig. 6(b)), the semicircle in the low-frequency region, which corresponds to  $R_{ct}$ , becomes larger with decreasing temperature.

Equivalent circuits from the TLM for the cylindrical pore model were used to obtain the quantitative internal resistance parameters from the experimentally recorded Nyquist plots at temperatures between -30°C and 60°C. As shown in Fig. 5, the impedance profiles

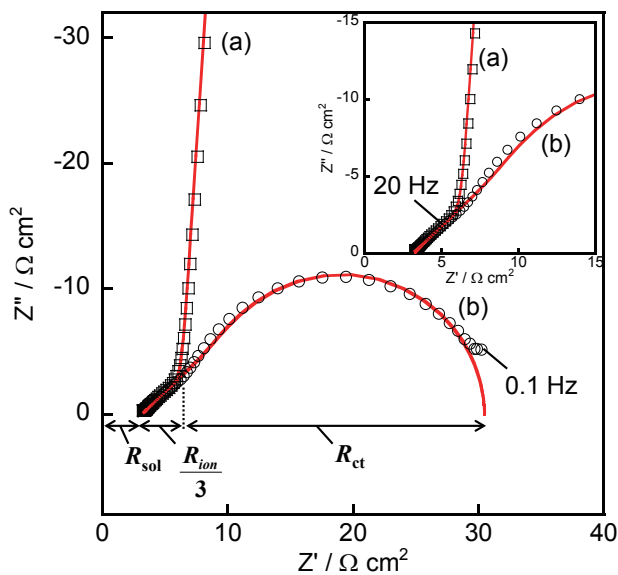


**Fig. 5** Nyquist plots for symmetric cells using two positive electrodes in 1.0 M LiPF<sub>6</sub> in EC/DMC/EMC (30/40/30) at 20°C. Electrodes prepared at: (a) SOC = 0% (squares) and (b) SOC = 50% (circles). The solid lines are the best-fit results with the equivalent circuits using Eqs. (1) and (2), for (a) and (b), respectively.

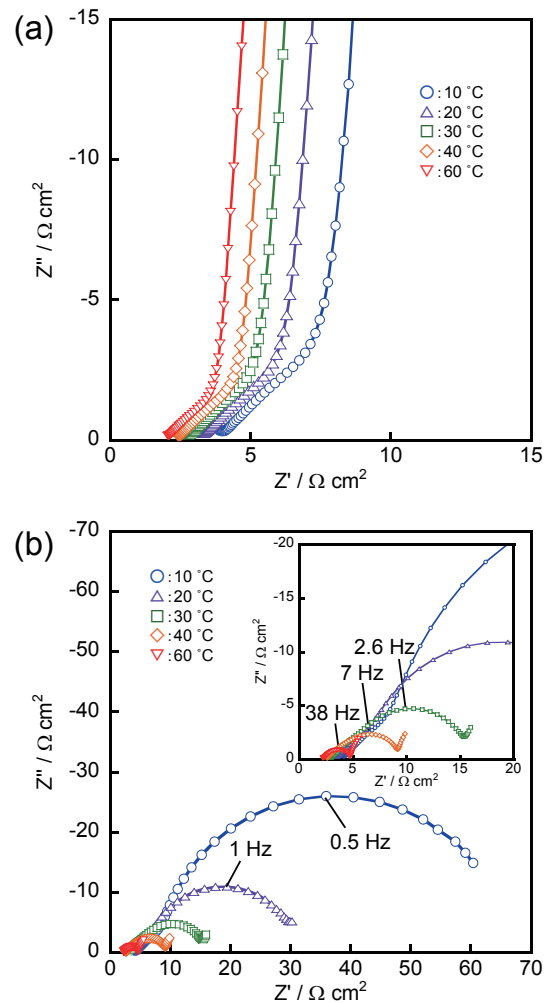


**Fig. 6** Nyquist plots for symmetric cells using two positive electrodes at (a) SOC = 0% and (b) 50% in 1.0 M LiPF<sub>6</sub> in EC/DMC/EMC (30/40/30) at various temperatures.



fit well with the equivalent circuits using Eqs. (1) and (2); therefore,  $R_{\text{sol}}$ ,  $R_{\text{ion}}$ , and  $R_{\text{ct}}$  can be obtained separately from the Nyquist plots of Fig. 6 as well. The inverse of the internal resistances obtained by fitting is plotted as a function of temperature in Fig. 7. For the EIS measurements of  $R_e$  (Fig. 3(b)), two identical electrodes were assembled in direct contact (e.g., positive-positive electrodes) without the separator (electrically non-blocking condition).  $R_e$  is smaller by 2-4 orders of magnitude when compared with other internal resistances, and can therefore be ignored.  $R_{\text{ion}}$  is larger than  $R_{\text{sol}}$ , but the temperature dependence of  $R_{\text{sol}}$  and  $R_{\text{ion}}$  is similar.  $R_{\text{ct}}$  is the largest of these four internal resistances for temperatures between room temperature and  $-30^\circ\text{C}$ . However,  $R_{\text{ct}}$  shows a strong temperature dependence and becomes smaller than  $R_{\text{sol}}$  and  $R_{\text{ion}}$  above room temperature.

To determine the kinetic parameters of interfacial phenomena at porous electrodes for faradaic processes, the activation energies of each resistance ( $R_x$ ) were evaluated using the Arrhenius equation,

$$\frac{1}{R_x} = A \exp\left(-\frac{E_a}{RT}\right), \quad (8)$$

where  $A$ ,  $E_a$ ,  $R$ , and  $T$  are the frequency factor, activation energy, gas constant, and absolute temperature, respectively. All internal resistances display Arrhenius behavior, as shown in Fig. 7. The activation energies for the individual internal resistances are calculated from Eq. (8) and are listed in the inset table of Fig. 7. The activation energies for  $R_{\text{sol}}$  ( $14.9 \text{ kJ mol}^{-1}$ ) and  $R_{\text{ion}}$  ( $16.3 \text{ kJ mol}^{-1}$ ) are similar; therefore, the activation energies for  $R_{\text{sol}}$  and  $R_{\text{ion}}$  are reflective of similar lithium-ion conduction (or transport) in the bulk electrolyte and in the electrolyte-filled pores, respectively. The activation energy for  $R_{\text{ct}}$  ( $57.6 \text{ kJ mol}^{-1}$ ) is higher than those of other resistances. This large value is consistent with previous reports that lithium-ion transfer at several solid/liquid interfaces is affected by lithium-ion desolvation.<sup>(26,27)</sup> Thus, a higher kinetic barrier exists at the solid/liquid interface than exists for moving from the electrolyte bulk to electrolyte inside the pore. Simple comparison of the internal resistance components at porous positive electrodes reveals that the ordering of the activation energies is as follows:  $E_{a, \text{ct}} > E_{a, \text{ion}} \approx E_{a, \text{sol}} \gg E_{a, e}$ .

## 5. Conclusions

In this paper, the individual internal resistance components of a porous electrode/electrolyte interface have been investigated in detail by combining the transmission line model (TLM) theory for cylindrical pores with electrochemical impedance spectroscopy using symmetric cells (EIS-SC). We have succeeded in separating four internal resistances at the porous electrode as the following parameters:  $R_e$ ,  $R_{\text{sol}}$ ,  $R_{\text{ion}}$ , and  $R_{\text{ct}}$ . The results show that despite its simplicity, the approach provides reasonably accurate results and is sufficient for analysis of the electrochemical characteristics of actual porous electrodes for lithium-ion batteries.

## References

- (1) Doyle, M., Meyers, J. P. and Newman, J., "Computer Simulations of the Impedance Response of Lithium Rechargeable Batteries", *J. Electrochem. Soc.*, Vol. 147, No. 1 (2000), pp. 99-110.

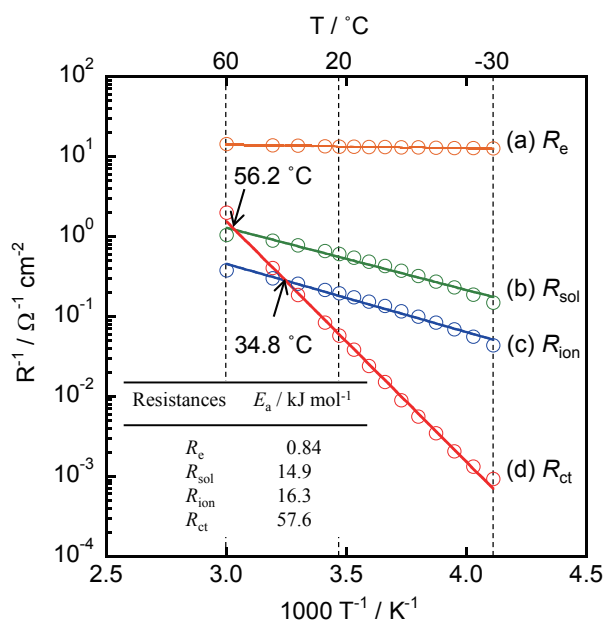


**Fig. 7** Temperature dependence of each internal resistance: (a) electric resistance ( $R_e$ ), (b) electrolyte bulk resistance ( $R_{\text{sol}}$ ), (c) ionic resistance in pores ( $R_{\text{ion}}$ ), and (d) charge-transfer resistance of lithium intercalation reaction ( $R_{\text{ct}}$ ). These resistances were obtained by fitting the data of Fig. 6 with Eqs. (1) and (2). Inset: activation energy of each internal resistance.

- (2) Meyers, J. P., Doyle, M., Darling, R. M. and Newman, J., "The Impedance Response of a Porous Electrode Composed of Intercalation Particles", *J. Electrochem. Soc.*, Vol. 147, No. 8 (2000), pp. 2930-2940.
- (3) Devan, S., Subramanian, V. R. and White, R. E., "Analytical Solution for the Impedance of a Porous Electrode", *J. Electrochem. Soc.*, Vol. 151, No. 6 (2004), pp. A905-A913.
- (4) Qu, D. Y. and Shi, H., "Studies of Activated Carbons Used in Double-layer Capacitors", *J. Power Sources*, Vol. 74, No. 1 (1998), pp. 99-107.
- (5) Song, H. K., Jung, Y. H., Lee, K. H. and Dao, L. H., "Electrochemical Impedance Spectroscopy of Porous Electrodes: the Effect of Pore Size Distribution", *Electrochim. Acta*, Vol. 44, No. 20 (1999), pp. 3513-3519.
- (6) Jang, J. H. and Oh, S. M., "Complex Capacitance Analysis of Porous Carbon Electrodes for Electric Double-layer Capacitors", *J. Electrochem. Soc.*, Vol. 151, No. 4 (2004), pp. A571-A577.
- (7) Jang, J. H., Yoon, S., Ka, B. H., Jung, Y. H. and Oh, S. M., "Complex Capacitance Analysis on Leakage Current Appearing in Electric Double-layer Capacitor Carbon Electrode", *J. Electrochem. Soc.*, Vol. 152, No. 7 (2005), pp. A1418-A1422.
- (8) Itagaki, M., Suzuki, S., Shitanda, I., Watanabe, K. and Nakazawa, H., "Impedance Analysis on Electric Double Layer Capacitor with Transmission Line Model", *J. Power Sources*, Vol. 164, No. 1 (2007), pp. 415-424.
- (9) Itagaki, M., Hatada, Y., Shitanda, I. and Watanabe, K., "Complex Impedance Spectra of Porous Electrode with Fractal Structure", *Electrochim. Acta*, Vol. 55, No. 21 (2010), pp. 6255-6262.
- (10) Taberna, P. L., Simon, P. and Fauvarque, J. F., "Electrochemical Characteristics and Impedance Spectroscopy Studies of Carbon-carbon Supercapacitors", *J. Electrochem. Soc.*, Vol. 150, No. 3 (2003), pp. A292-A300.
- (11) Los, P., Lasia, A., Menard, H. and Brossard, L., "Impedance Studies of Porous Lanthanum-Phosphate-bonded Nickel Electrodes in Concentrated Sodium-hydroxide Solution", *J. Electroanal. Chem.*, Vol. 360, No. 1-2 (1993), pp. 101-118.
- (12) Hitz, C. and Lasia, A., "Experimental Study and Modeling of Impedance of the Her on Porous Ni Electrodes", *J. Electroanal. Chem.*, Vol. 500, No. 1-2 (2001), pp. 213-222.
- (13) Recham, N., Chotard, J. N., Dupont, L., Delacourt, C., Walker, W., Armand, M. and Tarascon, J. M., "A 3.6 V lithium-based Fluorosulphate Insertion Positive Electrode for Lithium-ion Batteries", *Nat. Mater.*, Vol. 9, No. 1 (2010), pp. 68-74.
- (14) Okumura, T., Fukutsuka, T., Matsumoto, K., Orikasa, Y., Arai, H., Ogumi, Z. and Uchimoto, Y., "Lithium-ion Transfer Reaction at the Interface between Partially Fluorinated Insertion Electrodes and Electrolyte Solutions", *J. Phys. Chem. C*, Vol. 115, No. 26 (2011), pp. 12990-12994.
- (15) Nayak, P. K., Grinblat, J., Levi, M., Markovsky, B. and Aurbach, D., "Structural and Electrochemical Evidence of Layered to Spinel Phase Transformation of Li and Mn Rich Layered Cathode Materials of the Formulae  $x\text{Li}[\text{Li}_{1/3}\text{Mn}_{2/3}]\text{O}_2 \cdot (1-x)\text{LiMn}_{1/3}\text{Ni}_{1/3}\text{Co}_{1/3}\text{O}_2$  ( $x = 0.2, 0.4, 0.6$ ) upon Cycling", *J. Electrochem. Soc.*, Vol. 161, No. 10 (2014), pp. A1534-A1547.
- (16) Zhou, J., Li, R., Fan, X., Chen, Y., Han, R., Li, W., Zheng, J., Wang, B. and Li, X., "Rational Design of a Metal-organic Framework Host for Sulfur Storage in Fast, Long-cycle Li-S Batteries", *Energy Environ. Sci.*, Vol. 7, No. 8 (2014), pp. 2715-2724.
- (17) Ogihara, N., Kawauchi, S., Okuda, C., Itou, Y., Takeuchi, Y. and Ukyo, Y., "Theoretical and Experimental Analysis of Porous Electrodes for Lithium-Ion Batteries by Electrochemical Impedance Spectroscopy Using a Symmetric Cell", *J. Electrochem. Soc.*, Vol. 159, No. 7 (2012), pp. A1034-A1039.
- (18) Ogihara, N., Itou, Y., Sasaki, T. and Takeuchi, Y., "Impedance Spectroscopy Characterization of Porous Electrodes under Different Electrode Thickness Using a Symmetric Cell for High-performance Lithium-Ion Batteries", *J. Phys. Chem. C*, Vol. 119, No. 9 (2015), pp. 4612-4619.
- (19) de Levie, R., "On Porous Electrodes in Electrolyte Solutions", *Electrochim. Acta*, Vol. 8, No. 10 (1963), pp. 751-780.
- (20) de Levie, R., "On Porous Electrodes in Electrolyte Solutions—IV", *Electrochim. Acta*, Vol. 9, No. 9 (1964), pp. 1231-1245.
- (21) Bisquert, J., "Influence of the Boundaries in the Impedance of Porous Film Electrodes", *Phys. Chem. Chem. Phys.*, Vol. 2, No. 18 (2000), pp. 4185-4192.
- (22) Hansen, C. P. and Bertelsen, S., "Boerhaave's Syndrome: Spontaneous Rupture of the Oesophagus", *Ann Chir Gynaecol.*, Vol. 77, No. 4 (1988), pp. 138-141.
- (23) Barcia, O. E., D'Elia, E., Frateur, I., Mattos, O. R., Pébère, N. and Tribollet, B., "Application of the Impedance Model of de Levie for the Characterization of Porous Electrodes", *Electrochim. Acta*, Vol. 47, No. 13-14 (2002), pp. 2109-2116.
- (24) Bisquert, J., Gratzel, M., Wang, Q. and Fabregat-Santiago, F., "Three-channel Transmission Line Impedance Model for Mesoscopic Oxide Electrodes Functionalized with a Conductive Coating", *J. Phys. Chem. B*, Vol. 110, No. 23 (2006), pp. 11284-11290.

- (25) Itagaki, M., Suzuki, S., Shitanda, I. and Watanabe, K.,  
 “Electrochemical Impedance and Complex Capacitance to Interpret Electrochemical Capacitor”,  
*Electrochemistry*, Vol. 75, No. 8 (2007), pp. 649-655.
- (26) Yamada, I., Abe, T., Iriyama, Y. and Ogumi, Z.,  
 “Lithium-ion Transfer at  $\text{LiMn}_2\text{O}_4$  Thin Film Electrode Prepared by Pulsed Laser Deposition”,  
*Electrochem. Commun.*, Vol. 5, No. 6 (2003), pp. 502-505.
- (27) Yamada, Y., Iriyama, Y., Abe, T. and Ogumi, Z.,  
 “Kinetics of Lithium Ion Transfer at the Interface between Graphite and Liquid Electrolytes: Effects of Solvent and Surface Film”,  
*Langmuir*, Vol. 25, No. 21 (2009), pp. 12766-12770.

Figs. 1, 3, 5-7

Reprinted from *J. Electrochem. Soc.*, Vol. 159, No. 7 (2012), pp. A1034-A1039, Ogihara, N., Kawauchi, S., Okuda, C., Itou, Y., Takeuchi, Y. and Ukyo, Y., Theoretical and Experimental Analysis of Porous Electrodes for Lithium-ion Batteries by Electrochemical Impedance Spectroscopy Using a Symmetric Cell, © 2012 The Electrochemical Society.

Fig. 2

Reprinted from *J. Phys. Chem. C*, Vol. 119, No. 9 (2015), pp. 4612-4619, Ogihara, N., Itou, Y., Sasaki, T. and Takeuchi, Y., Impedance Spectroscopy Characterization of Porous Electrodes under Different Electrode Thickness Using a Symmetric Cell for High-performance Lithium-ion Batteries, © 2015 ACS Publications.

---

### Nobuhiro Ogihara

Research Fields:

- Electrochemistry
- Energy Storage Devices

Academic Degree: Ph.D.

Academic Societies:

- The Electrochemical Society of Japan
- The Electrochemical Society




---

### Yuichi Itou

Research Fields:

- Battery Materials and Processing
- Electrochemistry

Academic Societies:

- The Electrochemical Society of Japan
- The Japanese Society for Non-destructive Inspection

Award:

- Best Paper Award, the Japanese Society for Non-destructive Inspection, 1996

